ACS APPLIED NANO MATERIALS

www.acsanm.org

Forum Article

Nanozyme–Cellulose Hydrogel Composites Enabling Cascade Catalysis for the Colorimetric Detection of Glucose

Roberto Baretta, Valeria Gabrielli, and Marco Frasconi*

Cite This: *ACS Appl. Nano Mater.* 2022, 5, 13845–13853

Read Online

ACCESS | Metrics & More | Article Recommendations | Supporting Information

ABSTRACT: Catalytic cascades obtained from the combination of nanozymes, which are nanomaterials with enzyme-like activity, and natural enzymes have drawn much attention for biosensing and biomedical applications. A key consideration in the development of cascade reaction systems is the integration of nanozymes with enzymes to boost the overall catalytic performance. Here, we report an efficient one-pot approach for the preparation of an enzyme–nanozyme hydrogel composite for cascade catalysis. Prussian blue (PB) nanoparticles (NPs) were prepared by using mild synthetic conditions in a cellulose-based hydrogel network in the presence of glucose oxidase (GOx), resulting in the simultaneous immobilization of PB NPs and active GOx in the hydrogel. This integrated system not only displays peroxidase-like activity relative to the PB NPs but also reveals an enhanced cascade catalytic performance for the colorimetric detection of glucose due to the proximity effect of the enzyme–nanozyme system within the hydrogel matrix. Compared to the analogue mixture with GOx in solution, the composite hydrogel shows enhanced glucose detection and improved stability. The developed colorimetric assay was successfully applied for the analysis of glucose in human serum samples, demonstrating its potential in clinical diagnosis. The versatility of this one-pot protocol holds promise for the development of different multienzyme systems, leading to efficient cascade catalysis for sensing applications.

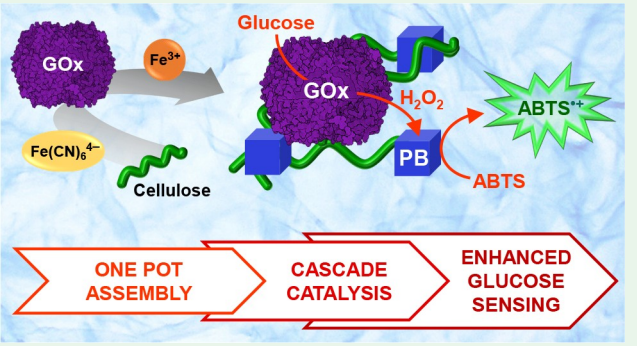

KEYWORDS: *biomimetic catalysis, MOF, sensing platforms, hydrogen peroxide, nanoparticles*

1. INTRODUCTION

Biological systems are characterized by complex cascade reactions, which are regulated by the spatial organization of enzymes in confined subcellular compartments.[1] The development of synthetic analogues of natural enzymes confined in nano/microenvironments for catalytic cascades has attracted a large amount of research attention.[2] Developing robust biomimetic catalysts aims also to expand the applications of enzymes, which are limited by high cost, low stability, and easy inactivation. The progress made so far in the realm of nanotechnology to fabricate nanomaterials with enzyme-like activity, the nanozymes,[3] holds significant promises. A variety of nanoparticles (NPs), including noble metals,[4,5] transition-metal oxides,[6,7] carbon dots,[8,9] and metal–organic frameworks (MOFs),[10−12] have been shown to mimic the catalytic activity of enzymes,[2] also exhibiting high pH and temperature tolerance compared to natural enzymes.[6] Among them, MOFs, which are crystalline porous nanomaterials based on inorganic ions cross-linked by multidentate organic ligands, have aroused tremendous interest because of their large variety of functionality, large and accessible specific surface areas, and defined pore sizes. In addition, their catalytic activity can be finely tuned by different ligands and postmodifications of the MOF surface.[10,11] Integrated multienzyme systems were prepared by the immobilization of natural enzymes, such as glucose oxidase (GOx), within the rigid scaffold of MOF exhibiting peroxidase-like activity.[12−14] Confinement of the enzyme in the MOF nanozyme resulted in cascade enzymatic reactions, which have been successfully employed for the detection of glucose.

On the other hand, in biological systems, the catalytic activity and selectivity of enzymes are tuned by folding of the soft polypeptide scaffold around the binding pocket, while their spatial organization in confined subcellular compartments enables effective cascade reactions.[1] The engineering of nanozymes with soft polymer scaffolds, mimicking the ability of a polypeptide to protect the catalytic center of enzymes and avoid undesired reactions, would provide a better biocompatibility of nanozymes for biomedical applications.[15] Different

Special Issue: Professor Sir Fraser Stoddart's 80th Birthday Forum

Received: April 13, 2022
Accepted: June 2, 2022
Published: June 27, 2022

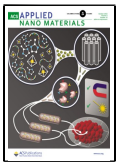

strategies have been employed for the immobilization and stabilization of nanozymes within a polymeric scaffold, by chemical grafting of the polymer to the nanozyme or by its physical entrapment in the polymer network.[16−20] The postsynthetic modification of nanozymes with hydrophilic polymers has enabled the development of hydrogel-coated nanozymes, with enhanced stability in biological media.[18]

Indeed, hydrogels can provide a suitable porous scaffold for nanozyme immobilization and protection from coalescence phenomena and from the nonspecific adsorption of biomacromolecules on the nanozyme surface.[21,22] Nanozyme−hydrogel composites are therefore poised to become invaluable catalytic tools for a huge variety of applications, including bioanalysis, drug delivery, and diagnosis, because of their high water retention capacity and adaptability to the biological environment.[23,24] In addition, the high loading capacity of hydrogel networks would allow the combined immobilization of nanozymes and natural enzymes.[21,25] The network structure of the hydrogel would provide a confined environment for communication between the two catalysts for operating catalytic cascade reactions. The challenges associated with the preparation of this multienzyme-integrated system include, among others, the ability to maintain the enzymatic activity during preparation of the hydrogel composite by using mild synthetic conditions, which is difficult to achieve with the common procedures for the synthesis of nanozymes.

Here, we present a one-pot assembly procedure for the preparation of an enzyme-nanozyme cascade platform by integrating Prussian blue (PB) NPs and GOx within a cellulose-based hydrogel. PB NPs are composed of Fe atoms in two different oxidation states coordinated by cyanide bridges,[26] and they exhibit outstanding catalase and peroxidase-like catalytic activity.[27−29] They have been employed in combination with chromogenic substrates for the detection of hydrogen peroxide (H_2O_2) and, by coupling with GOx, for the development of colorimetric glucose sensors.[28,30,31] Because of their excellent biocompatibility, PB NPs have recently emerged as a promising nanomaterial for biomedical applications.[32−36] The preparation of PB NPs by the coprecipitation method results in nanocrystals with large surface areas, whose dimensions can be tuned by using surface capping agents, such as poly(vinylpyrrolidone) (PVP).[37,38] However, these methods are usually performed at high temperatures (i.e., 80 °C) and involve solvents, such as ethanol/water mixtures,[37] which are not suitable for the entrapment of natural enzymes within the polymer matrix during the preparation of PB nanocomposites. Recently, PB NPs were prepared in aqueous media by cross-linking Fe^{3+} ions, a precursor of the PB synthesis, in a carboxymethyl cellulose (CMC) nanofibril membrane, followed by the reaction with hexacyanoferrate at room temperature.[39] The resulting stiff cellulose-based membrane with embedded PB NPs was applied as a filter for the removal of cesium from wastewater. Although the procedure employed mild conditions, the synthesis of PB NPs involved two steps; in particular, the initial formation of a highly coordinated hydrogel precludes from the possibility of embedding enzymes in the matrix.

Herein, we report a new strategy for the synthesis of PB NPs via the *in situ* precipitation in a CMC-based hydrogel network and the embedding of GOx in one step. CMC is a cellulose derivative with substituent carboxymethyl groups that possesses excellent biocompatibility, high water solubility, and chelating properties.[40] Thanks to its ability to coordinate metal cations,[41] CMC-based hydrogels have been employed as smart bioinks for 3D bioprinting applications.[42] Biocompatible optical fibers fabricated from a CMC-based hydrogel cross-linked with Al^{3+} ions were recently developed for sensing applications,[43] with the potential for *in vivo* biological sensing. Among the salient features of CMC, sensing interfaces modified with CMC were observed to inhibit nonspecific protein adsorption,[44,45] which is an important problem that negatively affects the performance of biosensors. Indeed, the nonspecific adsorption of proteins from complex biological samples, such as serum, can reduce binding of the analyte to the active site for its detection, decreasing the sensitivity and reproducibility of the sensor.[46] Therefore, CMC was chosen as a scaffold for the preparation of our integrated nanozyme−enzyme hydrogel composite, leading to an efficient and reliable platform for the detection of glucose in real samples. In our hydrogel-mediated strategy, CMC acts as a capping agent to control the growth of PB NPs and as an immobilization matrix for the PB NPs and enzyme. The hydrogel composite obtained by the cross-linking of CMC with PB NPs results in the efficient immobilization of active GOx thanks to enhanced swelling of the CMC-based hydrogel. The integrated platform exhibits an enhanced cascade catalytic performance, achieving superior sensitivity for the colorimetric detection of glucose with respect to the free enzyme in solution because of the proximity effect of the enzyme−nanozyme system within the hydrogel matrix. The ability of the CMC-based hydrogel to stabilize the PB NPs within the matrix and protect the enzyme from degradation provided an assay with high stability. To demonstrate the feasibility of our colorimetric assay for real sample analysis, the developed platform was used for the determination of glucose in human serum samples. Because of its facile preparation, stability, and versatility, our approach holds great promise for the development of different multienzyme systems, leading to efficient cascade catalysis for sensing applications.

2. EXPERIMENTAL SECTION

2.1. Materials and Chemicals. Sodium carboxymethyl cellulose (NaCMC; MW = 250 kDa, DS = 0.9), iron(III) nitrate nonahydrate [$Fe(NO_3)_3{\cdot}9H_2O$; 98%], potassium hexacyanoferrate(II) trihydrate [$K_4Fe(CN)_6{\cdot}3H_2O$; 98.5%], 30% (w/w) hydrogen peroxide (H_2O_2) solution, sodium phosphate dibasic dihydrate (99%), sodium phosphate monobasic dihydrate (99%), ethylenediaminetetraacetic acid disodium salt dihydrate (EDTA; 99%), D-glucose (99.5%), 2,2′-azinobis(3-ethylbenzothiazolinesulfonic acid) diammonium salt (ABTS; 98%), glucose oxidase from *Aspergillus niger* (GOx; 145 U/mg), and horseradish peroxidase (HRP; 200 U/mg) were all purchased from Sigma-Aldrich Co. (St. Louis, MO). 2-(*N*-Morpholino)ethanesulfonic acid monohydrate (MES; 99%) was purchased from Fluka Chemie GmbH.

2.2. Instrumentation. Ultraviolet−visible (UV−vis) spectra were collected using an Agilent Cary 60 spectrophotometer. Fourier transform infrared (FTIR) spectra were obtained with a Nicolet Nexus 670 FTIR spectrometer. Scanning electron microscopy (SEM) with energy-dispersive X-ray spectroscopy (EDX) images were taken on a Zeiss Sigma HD microscope, equipped with a Schottky field-emission-gun source, one detector for backscattered electrons, and two detectors for secondary electrons (InLens and Everhart Thornley). Transmission electron microscopy (TEM) images were taken on a Tecnai G^2 (FEI) operating at 100 kV. Images were captured with a Veleta (Olympus Soft Imaging System) digital camera. X-ray diffraction (XRD) patterns were recorded on a Bruker D8 ADVANCE Plus diffractometer in Bragg−Brentano geometry employing Cu Kα line radiation.

https://doi.org/10.1021/acsanm.2c01609
ACS Appl. Nano Mater. 2022, 5, 13845−13853

Scheme 1. Schematic Representation of the Synthetic Approach for the Preparation of PB−CMC Hydrogel Composite and the Corresponding Catalyzed Oxidation of ABTS with H_2O_2

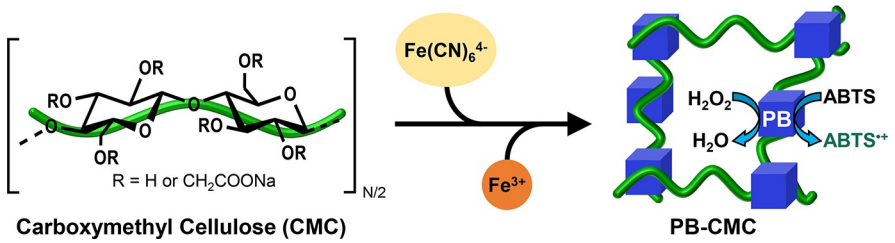

2.3. Preparation of PB−CMC. NaCMC (40.0 mg) was dissolved homogeneously in deionized (DI) water (2 mL), and a solution of $K_4Fe(CN)_6{\cdot}3H_2O$ (150 mM, 100 μL) was added. Subsequently, a solution of $Fe(NO_3)_3{\cdot}9H_2O$ (10 mM, 2 mL) was added dropwise under vigorous magnetic stirring, and the resulting suspension was stirred continuously for 5 min at room temperature. The final concentrations in the reaction mixture were 1% (w/w) CMC, 3.75 mM $Fe(CN)_6^{4-}$, and 5 mM Fe^{3+}. Next, 1.0 mL of water was added, and the reaction mixture was centrifugated for 3 min at 8300 rpm. The supernatant was removed, and the collected blue hydrogel was redispersed in 2.5 mL of 10 mM MES buffer (pH 5.05).

2.4. Preparation of PB−CMC−GOx. GOx embedded in a PB−CMC composite (PB−CMC−GOx) was prepared according to the above method with the addition of 100 μL of a 6.0 mg/mL GOx solution to the solution of $K_4Fe(CN)_6{\cdot}3H_2O$ and NaCMC. The final concentration of GOx in the reaction mixture was 0.15 mg/mL. The subsequent step for the *in situ* synthesis of PB NPs consisted of the dropwise addition of a $Fe(NO_3)_3{\cdot}9H_2O$ solution and washing of the resulting PB−CMC−GOx composite, as reported above for PB−CMC.

2.5. Evaluation of the Peroxidase-Mimicking Activity of PB−CMC. The catalytic activity of the prepared PB−CMC composite toward H_2O_2 was evaluated by using ABTS as a chromogenic substrate. In a typical experiment, 500 μL of a PB−CMC suspension and 250 μL of ABTS (4.0 mM) were added into a MES buffer (10 mM, pH 5.05) to a total volume of 2.0 mL. Variable concentrations of H_2O_2 were added, in order to obtain concentrations in the cuvette between 2.0 and 50.0 μM. The catalytic oxidation of ABTS was followed by UV−vis spectroscopy by measuring the absorbance changes at a wavelength of 420 nm.

2.6. Colorimetric Detection of Glucose Using PB−CMC−GOx. The cascade reaction of GOx and PB NPs within the PB−CMC−GOx integrated system was evaluated in the presence of glucose and ABTS. For a typical colorimetric detection of glucose, 500 μL of a PB−CMC−GOx suspension and 250 μL of ABTS (4.0 mM) were added into a 10 mM MES buffer (pH 5.05) to a total volume of 2.0 mL. Variable concentrations of glucose were added in the cuvette, in order to obtain final glucose concentrations between 5.0 and 100.0 μM. The catalytic cascade reaction was followed spectroscopically by measuring the absorbance at a wavelength of 420 nm. As a control experiment, glucose detection was performed by a PB−CMC composite with GOx free in solution. Briefly, 5.3 μL of GOx (1 mg/mL) was added in a cuvette in the presence of 500 μL of a PB−CMC composite. The subsequent steps were performed by using the same procedure as that described above.

The colorimetric detection of glucose by a PB−CMC−GOx-based assay was validated in five human serum samples provided by volunteers. For this assay, 500 μL of a PB−CMC−GOx suspension and 250 μL of ABTS (4.0 mM) were added into a 10 mM MES buffer (pH 5.05) to a total volume of 2.0 mL, followed by the addition of 20 μL of a human serum sample. The absorbance of the resulting mixture was measured at a wavelength of 420 nm after incubation for 80 min at 25 °C. The concentration of glucose for each sample was obtained from three independent assay runs. The performance of the reported PB−CMC−GOx-based assay for the determination of glucose in serum was validated by means of the hexokinase−glucose−6-phosphate dehydrogenase method.

2.7. Determination of the Content of PB NPs in Hydrogel Composites. The content of PB NPs in PB−CMC and PB−CMC−GOx hydrogel composites was determined by the following procedure: 2.0 mL of a hydrogel composite was added to 2.0 mL of a 100 mM phosphate buffer solution (PBS) at pH 7.00, and the resulting mixture was stirred for 24 h. The supernatant was separated by centrifugation at 10000 rpm for 10 min, and the solid PB NPs were washed with DI water and acetone and then vacuum-dried until a constant weight. The percentage of NPs in the composite hydrogel was calculated from the weight of the PB NPs with respect to the dry composite. The PB NPs contents in the PB−CMC and PB−CMC−GOx hydrogel composites were estimated to be 39% and 42%, respectively.

2.8. Determination of the Content of GOx in the PB−CMC−GOx Composite. The content of GOx in the PB−CMC−GOx system was determined by assaying the activity of GOx after dissolution of the PB NPs from the composite. A suspension (500 μL) of PB−CMC−GOx in 50 mM PBS at pH 7.00 was added to 500 μL of EDTA (20 mM), and the resulting mixture was stirred for 3 h. Then, 2.50 mL of ABTS (5 mM), 0.50 mL of glucose (55 mM), and 10 μL of a HRP solution (200 U/mL) were added. The absorbance changes at a wavelength of 725 nm were measured, and the activity of GOx, expressed in enzymatic units (1 U produces 1 μmol/min of H_2O_2 at 25 °C and pH 7.00), was determined according to a previous report.[47]

3. RESULTS AND DISCUSSION

The PB−CMC hydrogel composite was prepared by the reaction of ferrocyanide, $Fe(CN)_6^{4-}$, and Fe^{3+} ions within the CMC polymer network, as outlined in Scheme 1.

The initial concentration of CMC and the ratio between $Fe(CN)_6^{4-}$ and Fe^{3+} were first optimized in order to obtain a homogeneous and well-dispersed PB−CMC hydrogel composite. A sufficient concentration of CMC was necessary to establish a polysaccharide hydrogel matrix that enables the *in situ* growth of dispersed PB NPs. When a 1% CMC aqueous solution was mixed with increasing $Fe(CN)_6^{4-}$ concentrations, from 0 to 3.75 mM, followed by the addition of 5.0 mM Fe^{3+} ions, the reaction mixture turned from orange to blue (Figure S1). The orange color was due to the formation of a Fe−CMC hydrogel,[48] while increasing the ferrocyanide concentration provides the formation of PB NPs embedded within the hydrogel matrix. The quantitative formation of a PB−CMC composite was obtained with a $Fe(CN)_6^{4-}/Fe^{3+}$ ratio of 0.75, which corresponds to the stoichiometry of insoluble PB.[26] The PB NPs content was evaluated to be 39% of the dried PB−CMC composite. At lower $Fe(CN)_6^{4-}/Fe^{3+}$ ratios, greenish gels were obtained, which correspond to a mixture of orange Fe−CMC and blue PB−CMC hydrogels (Figure S1). The underlying process in this hydrogel-mediated route to the synthesis of PB NPs is the exchange of cross-linking units of the CMC chains, from the initial Fe^{3+} metal precursor to the PB NPs. Indeed, the hydrogel network resulting from CMC cross-linked by Fe^{3+} ions acts as a confined environment for

https://doi.org/10.1021/acsanm.2c01609
ACS Appl. Nano Mater. 2022, 5, 13845−13853

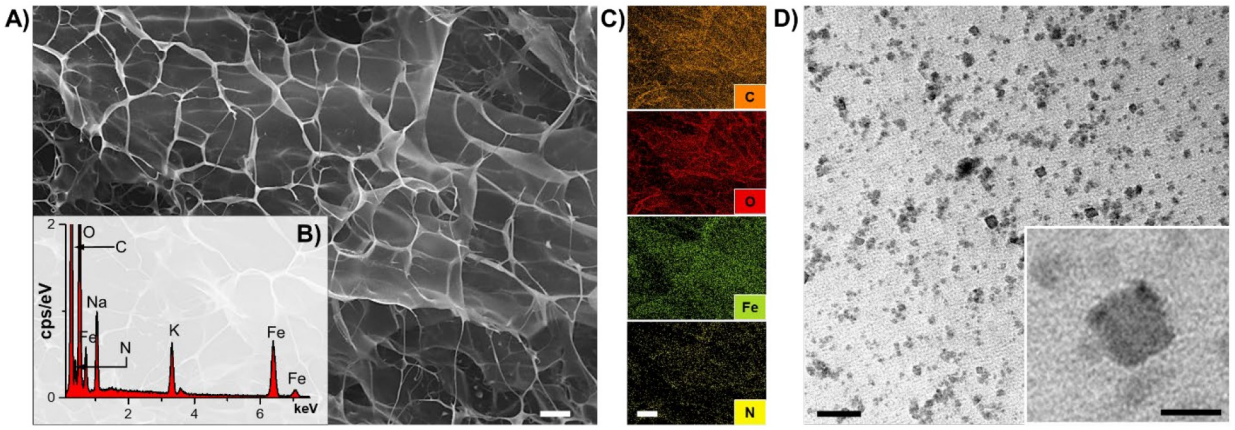

Figure 1. (A) SEM image (scale bar 20 μm), (B) EDX spectrum, and (C) EDX mapping images (scale bar 100 μm) of the lyophilized PB−CMC. (D) TEM images of PB−CMC (scale bar 100 nm). Inset: High-magnification image (scale bar 20 nm).

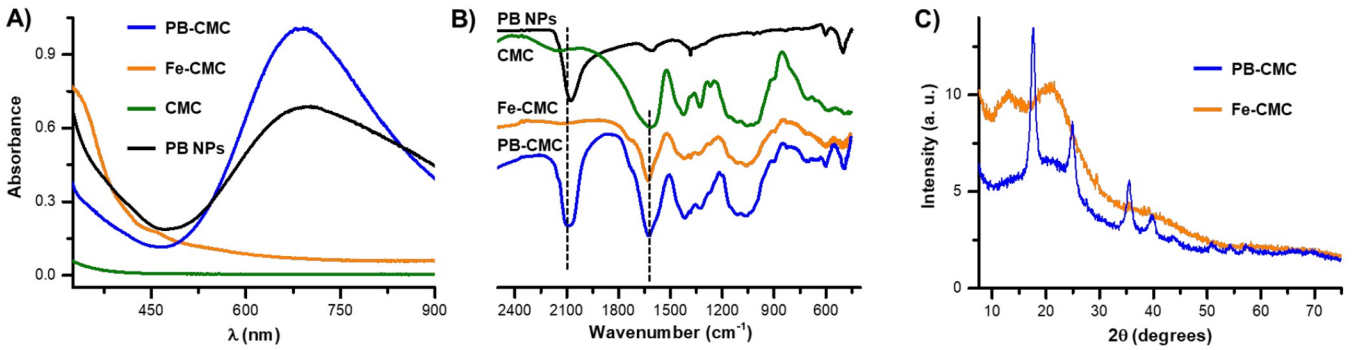

Figure 2. (A) UV−vis and (B) FTIR spectra of PB NPs (black), CMC (green), Fe−CMC (orange), and PB−CMC (blue). (C) PXRD patterns of lyophilized Fe−CMC (orange) and PB−CMC (blue).

the templated formation and growth of PB NPs. Therefore, increasing the $Fe(CN)_6^{4-}$ concentration in the reaction mixture to reach the optimal ratio resulted in the quantitative formation of PB NPs embedded within the CMC-based hydrogel.

The morphology of the prepared PB−CMC hydrogel composite was investigated by SEM. The lyophilized PB−CMC composite resulted in networks with regular pores on a scale of tens of microns (Figure 1A). On the contrary, the lyophilized Fe−CMC hydrogel exhibited a high density of small pore matrices (Figure S3), which is consistent with a higher degree of cross-linking by Fe^{3+} ions. EDX mapping of the PB−CMC composite displays (Figure 1C) a uniform distribution of C and O from CMC and of Fe, N, and K from PB, confirming its presence within the polymer matrix. The presence of K (Figure S2) indicates that PB NPs are present also in their soluble form, with K as the counterion.[26] Furthermore, the elemental mapping analysis of Fe−CMC revealed the presence of C, O, and Fe, consistent with Fe^{3+} ions cross-linking the cellulose-based hydrogel network (Figure S3).

Given the porous structure of the lyophilized PB−CMC, the PB NPs within the hydrogel cannot be observed by SEM. When PB−CMC is air-dried on a silicon substrate, SEM images clearly show the presence of PB NPs (Figure S4), as bright spots in the polymer scaffold. TEM images reveal that the PB NPs had a cubic shape and were uniformly dispersed in the hydrogel matrix (Figures 1D and S5). The size of the NPs was nearly 21 nm, which is smaller in comparison to those of PB NPs prepared by conventional methods, which typically have sizes in the range of 40−50 nm.[28,49] The possibility of obtaining such small PB NPs could be ascribed to stabilization of the CMC chains during preparation of the NPs. In order to evaluate the role of the CMC matrix during preparation of the PB−CMC composite, we performed the synthesis of PB NPs with the same concentrations of Fe^{3+} and $Fe(CN)_6^{4-}$ as those used for the preparation of PB−CMC but without CMC. The reaction resulted in a color change of the solution from yellow to blue, followed by a rapid precipitation of blue agglomerates. The SEM analysis shows that the predominant structures were irregularly shaped aggregates of about 60−200 nm (Figure S4). Therefore, the CMC matrix environment plays a critical role during the synthesis and growth of PB NPs and in their stabilization within the hydrogel.

The obtained PB−CMC hydrogel composite can be evenly dispersed in water at different ratios. The UV−vis spectrum of a dispersion of the as-synthesized PB−CMC in water (in the ratio 1:4) shows the characteristic broad absorption band of PB at 690 nm (Figure 2A). In a comparison of the spectrum of PB−CMC with that of PB NPs obtained without CMC, the absorption band of PB NPs shifts to a longer wavelength (710 nm). The red shift in the UV−vis spectrum could be ascribed to the formation of large particles and aggregates of PB for the synthesis without CMC, as confirmed by SEM (Figure S4). This is consistent with the previously reported phenomenon showing a red shift of the UV−vis spectrum for increasing PB NPs sizes.[33] Thus, the PB NPs obtained within the CMC network are smaller than those obtained without the polymer

https://doi.org/10.1021/acsanm.2c01609
ACS Appl. Nano Mater. 2022, 5, 13845−13853

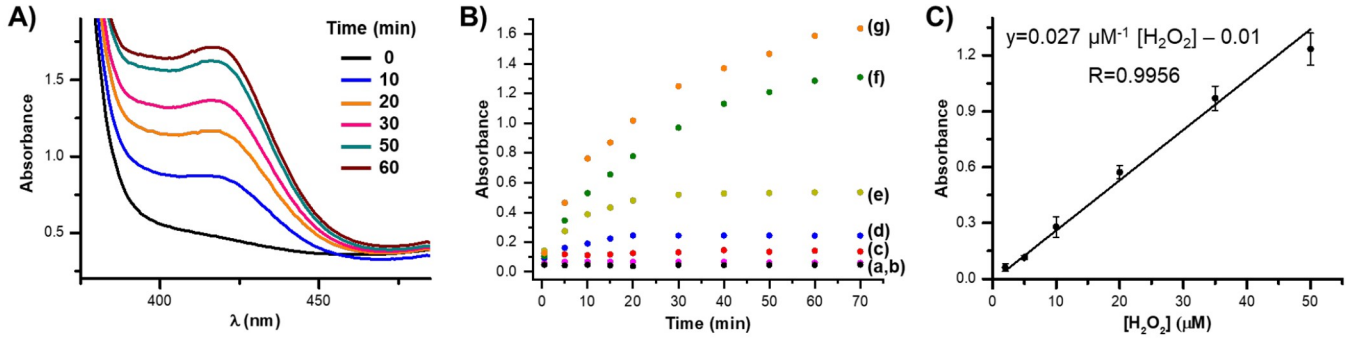

Figure 3. (A) UV−vis spectra of the ABTS oxidation reaction with 35 μM H_2O_2 catalyzed by PB−CMC. (B) Time-dependent absorbance changes upon ABTS oxidation catalyzed by PB−CMC with different concentrations (μM) of H_2O_2: (a) 0; (b) 2.0; (c) 5.0; (d) 10.0; (e) 20.0; (f) 35.0; (g) 50.0. (C) Linear calibration curve for H_2O_2 detection in the range of 2.0−50.0 μM. Error bars indicate the standard deviations from four measurements.

matrix, an observation that supports the role of CMC during the synthesis of PB NPs. The UV−vis spectrum of Fe−CMC hydrogel shows only a peak at 450 nm, which is characteristic of Fe^{3+} ions coordinated with carboxylic groups of the CMC chains.[50]

The FTIR spectra of the pure CMC, PB NPs, Fe−CMC, and PB−CMC dried samples are shown in Figure 2B. The spectra of PB NPs and PB−CMC show the characteristic peak attributed to the C≡N stretching of PB[51] at 2080 cm^{-1} and two peaks at 500 and 600 cm^{-1} characteristic of the Fe−C≡N−Fe bending of PB.[52] In addition, the spectrum of PB−CMC shows the characteristic COO^- asymmetric stretching peak of CMC. This peak is located at 1608 cm^{-1} for CMC, while it is shifted to 1628 cm^{-1} for both Fe−CMC and PB−CMC. We attributed this shift to the interaction of Fe^{3+} ions, in the Fe−CMC hydrogel, and PB NPs, in the PB−CMC hydrogel composite, with the COO^- groups of the CMC chains.[41] From the Fe−CMC and PB−CMC spectra, it is possible to observe a small shoulder at 1735 cm^{-1}, which is absent in the CMC spectrum, indicating that monodentate coordination occurs between COO^- and the cross-linkers, Fe^{3+} ions and PB NPs, respectively. All of these observations are consistent with coordination of the CMC chains by PB NPs, resulting in the PB−CMC hydrogel composite.

Insights into the formation of crystalline PB NPs were obtained by powder X-ray diffraction (PXRD). The diffraction pattern on Fe−CMC shows only broad bands typical of an amorphous cellulose-based material. PB−CMC shows (Figure 2C) diffraction peaks at 17.4°, 24.8°, 35.3°, 39.6°, 43.1°, 51.1°, 54.1°, 57.2°, 66.3°, and 68.4°, consistent with the characteristic peaks of crystalline PB.[53] The average dimensions of the crystallites within the PB−CMC composite were estimated, by using Scherrer's equation, to be around 8.2 nm. Taken together, these results support the crucial role of the interaction between the carboxylic groups of the CMC chains and PB NPs in the formation of the PB−CMC hydrogel network.

The enzyme-like catalytic activity of the PB NPs in the hydrogel composite was evaluated through the catalytic reduction of H_2O_2 in the presence of ABTS, as a peroxidase chromogenic substrate. The decomposition of H_2O_2 can therefore be monitored by UV−vis spectroscopy because of the oxidation of ABTS to the dark-green $ABTS^{\bullet+}$ product. The experimental conditions for the catalytic activity of the PB−CMC composite hydrogel were optimized by changing the concentrations of the catalyst and substrate and the pH of the solution. The pH−activity profile for ABTS oxidation by PB−CMC in the presence of H_2O_2 showed an optimum in the pH range of 4.5−5.5 and negligible activity at pH values above 7 (Figure S6), as a consequence of the instability of PB at even slightly alkaline pH values.[26] The UV−vis spectra generated by the presence of PB−CMC in a 10 mM MES buffer at pH 5.05 containing H_2O_2 and ABTS are shown in Figure 3A. An increase of the absorption band at 420 nm with the reaction time is observed, confirming the peroxidase-like activity of PB−CMC. The time-dependent absorbance changes upon oxidation of a fixed concentration of ABTS in the presence of different concentrations of H_2O_2 and a fixed amount of the PB−CMC composite are shown in Figure 3B. As the concentration of H_2O_2 increased, the catalytic oxidation of ABTS intensified. The calibration curve corresponding to the absorbance for a reaction time of 30 min is displayed in Figure 3C. The linearity range is from 2.0 to 50.0 μM H_2O_2, with a limit of detection (LOD) of 1.0 μM. Control experiments revealed that ABTS is not oxidized in the absence of PB−CMC or in the presence of PB−CMC but without H_2O_2 (Figure S7). It should be noted that the Fe−CMC hydrogel leads to a very inefficient oxidation of ABTS with H_2O_2 (Figure S7) because of the dissolution of Fe−CMC by H_2O_2 as a consequence of the Fenton reaction. The Fenton reaction is based on the Fe^{3+}-catalyzed decomposition of H_2O_2 to radicals,[54] which provide only a slight contribution to the oxidation of ABTS.

The steady-state kinetics for the catalytic reduction of H_2O_2 by the PB−CMC hydrogel composite in the presence of ABTS, followed the typical Michaelis−Menten model (Figure S8A). The values of the Michaelis−Menten constant (K_m) and maximum reaction velocity (V_{max}) obtained from the Lineweaver−Burk double reciprocal plot (Figure S8B) were 0.46 mM and 0.35 μM s^{-1}, respectively. Compared to HRP (3.70 mM)[6] and other PB NPs reported in the literature,[27] our value of K_m was smaller, indicating a higher affinity of PB−CMC for H_2O_2. The obtained value of K_m falls between the values reported for PB NPs encapsulated in a MOF [MIL-101(Cr)] scaffold (1.06 mM)[55] and for ultrasmall PB NPs prepared using PVP as the surface capping agent (0.2 mM).[37] With respect to other nanozymes with peroxidase-like activity, the K_m value for NiPd NPs immobilized on a zeolitic imidazolate framework 8 (ZIF-8) was 0.89 mM,[12] while for platinum nanozymes entrapped in a poly(ethylene glycol) hydrogel, K_m was 2.26 mM.[56]

https://doi.org/10.1021/acsanm.2c01609
ACS Appl. Nano Mater. 2022, 5, 13845−13853

Scheme 2. Schematic Representation of the One-Pot Approach for the Preparation of GOx Embedded within the PB−CMC Hydrogel Composite and the Corresponding Catalytic Cascade Reaction for the Detection of Glucose by the PB−CMC−GOx Integrated System

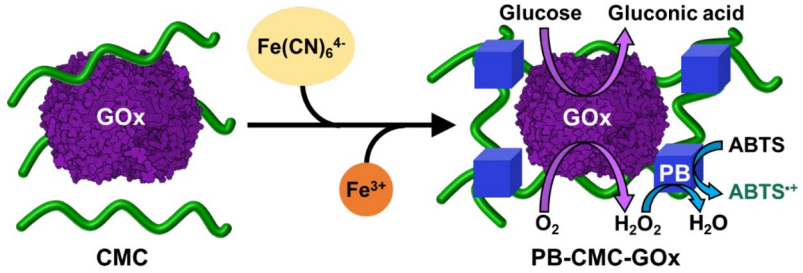

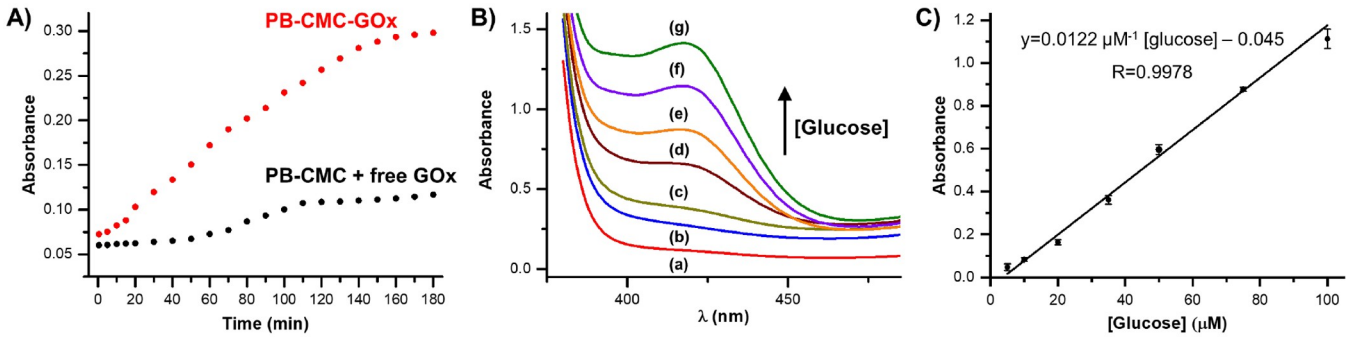

Figure 4. (A) Time-dependent absorbance changes upon ABTS oxidation with 20 μM glucose catalyzed by the PB−CMC−GOx integrated system (red curve) and by the PB−CMC composite with free GOx added in solution (black curve). (B) UV−vis spectra of the ABTS oxidation reaction catalyzed by PB−CMC−GOx after 80 min of reaction with different concentrations (μM) of glucose: (a) 5.0; (b) 10.0; (c) 20.0; (d) 35.0; (e) 50.0; (f) 75.0; (g) 100.0. (C) Linear calibration curve for glucose detection in the range of 5.0−100.0 μM. Error bars indicate the standard deviations from four measurements.

The PB−CMC hydrogel composite provides a colorimetric sensor for H_2O_2 with high stability and sensitivity. This suggests that the composite hydrogel could be used for cascade reactions with oxidase enzymes, such as GOx, which produces H_2O_2. Indeed, the colorimetric determination of H_2O_2 generated from the GOx catalytic oxidation by O_2 of glucose to gluconic acid provides a quantitative measure for glucose. To enable an efficient cascade reaction, the enzyme and nanozyme should operate within a confined microenvironment. Toward this goal, GOx was encapsulated within the hydrogel matrix during synthesis of the PB NPs in a one-step protocol according to Scheme 2. For the preparation of this integrated hydrogel composite, PB−CMC−GOx, where GOx and PB NPs are confined within the polymer network, the enzyme is loaded into the CMC matrix, followed by the addition of $Fe(CN)_6^{4-}$ and Fe^{3+} for the *in situ* synthesis of PB NPs. The color of the reaction mixture immediately turned blue, indicating the successful formation of PB NPs. The content of PB NPs in the dried PB−CMC−GOx composite was determined to be 42%, which is comparable to the content of PB NPs found in the PB−CMC composite.

The physicochemical properties of the resulting PB−CMC−GOx hydrogel composite were investigated and compared with those of the PB−CMC hydrogel. The SEM image of the lyophilized PB−CMC−GOx hydrogel shows (Figure S9) a porous matrix with a pore size similar to that of the PB−CMC hydrogel. The UV−vis spectrum of a water dispersion of the PB−CMC−GOx hydrogel is characterized (Figure S10) by an absorption band at a wavelength (690 nm) and an intensity similar to those observed for the PB−CMC hydrogel, confirming that the same amount of PB NPs is embedded in the CMC matrix for both hydrogel composites. The FTIR spectrum displays the characteristic peaks of PB at 500, 600, and 2080 cm^{-1}, confirming the presence of PB NPs in the newly synthesized PB−CMC−GOx composite. The PXRD pattern of PB−CMC−GOx shows the same diffraction peaks as those observed for the PB−CMC composite (Figure S11), confirming the formation of crystalline PB NPs. These results suggest that the syntheses of PB NPs and the resulting hydrogel composite are not significantly affected by the addition of the enzyme in the reaction environment.

The biocatalytic activity of GOx embedded in the PB−CMC−GOx composite was then evaluated. The optimized condition of pH 5.05 was adopted for the colorimetric detection of glucose by the PB−CMC−GOx composite (Figure S12). When glucose and ABTS were added to a 10 mM MES buffer (pH 5.05) containing the PB−CMC−GOx composite, the color of the solution turned dark green with a characteristic absorbance peak of $ABTS^{\bullet+}$ at 420 nm (Figure S13). This result highlights that GOx is embedded in the composite hydrogel in a catalytically active configuration, which oxidizes glucose with O_2 to locally produce H_2O_2, which is the substrate for the oxidation of ABTS by PB NPs. As a control, the addition of glucose and ABTS to a dispersion of PB−CMC does not result in any color change (Figure S13). The content of GOx embedded in the PB−CMC−GOx hydrogel was determined by colorimetric assay.[47] For this purpose, PB NPs were dissolved from the PB−CMC−GOx hydrogel by using EDTA as a chelating agent and then the enzymatic activity of GOx released in solution was assayed (see the Experimental Section for more details). The content of

https://doi.org/10.1021/acsanm.2c01609
ACS Appl. Nano Mater. 2022, 5, 13845−13853

GOx in the PB−CMC−GOx system was 1.5 ± 0.1 U/mL of hydrogel.

The proximity effect of GOx and PB NPs in the composite hydrogel is critical for the catalytic cascade because the H_2O_2 *in situ* generated by GOx would immediately react with PB NPs. In order to probe the cascade catalytic performance of the PB−CMC−GOx composite, we investigated the catalytic activity of the integrated system and compared to a mixture of PB−CMC and free GOx in solution. Figure 4A shows the time-dependent absorbance changes upon the addition of ABTS and glucose to the PB−CMC−GOx hydrogel composite and to the separated mixture of GOx and PB−CMC. The PB−CMC−GOx composite clearly exhibits an enhanced catalysis toward the cascade reactions compared to PB−CMC and free GOx, resulting in a higher sensitivity for glucose detection.

The analytical performance of the composite hydrogel for glucose detection was evaluated under the optimized conditions. Figure 4B shows the absorption spectra of the resulting $ABTS^{\bullet+}$ formed after a fixed time interval of 80 min, using fixed concentrations of ABTS and PB−CMC−GOx and variable concentrations of glucose. With an increase of the glucose concentration, the absorbance of the solution increased gradually. Figure 4C shows the derived calibration curve. A strong linear relationship between the absorbance, measured at 420 nm, and the content of glucose is observed in the concentration range of 5.0−100.0 μM, with a LOD of 1.0 μM. Compared to other glucose assays based on the integration of GOx and different nanozymes with peroxidase-like activity (Table S1), the proposed PB−CMC−GOx hydrogel composite presents a higher LOD and a comparable linear range. An important aspect relates to the stability of the PB−CMC−GOx hydrogel composite for the detection of glucose. We find that the assay retains up to 80% of its activity upon 1 month of storage at 4 °C in a 10 mM MES buffer at pH 5.05 (Figure S14A) and the characteristic absorption band of PB NPs at 690 nm does not change (Figure S14B), demonstrating the stability of GOx and nanozyme, respectively, in the hydrogel matrix. The good long-term storage stability of the PB−CMC−GOx composite can be ascribed to the CMC network, which provides good protection of the enzyme from degradation and excellent stabilization of the PB NPs, preventing its leakage in the solution.

In order to demonstrate the applicability of the PB−CMC−GOx system for the assay of glucose in real samples, the developed colorimetric platform was applied to determine glucose in human serum samples. Accordingly, the samples of human serum were 100-fold-diluted in the chromogenic mixture of PB−CMC−GOx and ABTS in a MES buffer (pH 5.05), and the concentration of glucose was determined from measurement of the absorbance at 420 nm.

The glucose levels obtained from our assay on five samples of serum are in good agreement with those obtained by the clinical method (Table 1), with a relative standard deviation ranging from 1.2 and 4.1%. Analysis of the samples with variable concentrations of glucose also revealed good precision of our method. Therefore, the developed assay can be effectively used for the quantification of glucose in clinically relevant samples.

Table 1. Determination of Glucose in Human Serum Samples

sample	this method (mM)	clinical method (mM)
1	4.2 ± 0.2	4.38
2	5.1 ± 0.3	5.20
3	6.7 ± 0.2	6.62
4	5.7 ± 0.1	5.81
5	4.1 ± 0.1	3.94

4. CONCLUSIONS

In summary, we have demonstrated a versatile one-pot strategy to fabricate an integrated enzyme−nanozyme system within a cellulose-based hydrogel. The hydrogel composite is based on cellulose, as a gelator, and crystalline PB NPs, which act both as a cross-linker for the hydrogel network and as a nanozyme exhibiting peroxidase-like activity. Formation of the CMC-based hydrogel network provides a biocompatible scaffold for the immobilization of GOx without affecting the catalytic activity of the enzyme. In addition, the hydrogel network acts as a confined environment for the enzyme and nanozyme to operate biocatalytic cascade reactions. The PB−CMC−GOx hydrogel composite revealed high sensitivity for the colorimetric detection of glucose, and compared with the mixture of separated GOx and PB−CMC, our integrated system shows enhanced glucose detection and improved stability. The developed colorimetric assay was validated for the determination of glucose in human serum samples, confirming the efficiency of our platform for real sample analysis. Importantly, the use of CMC-based hydrogels holds particular interest for the development of enzyme−nanozyme assays thanks to the ability of CMC to reduce unspecific protein absorption in real samples. Hence, because of the straightforward synthetic strategy of the PB−CMC−GOx hydrogel and its feasibility for the detection of glucose in complex biological media, our approach holds promise for future applications in clinical diagnosis. In addition, PB NPs embedded in biocompatible polymers, as the cellulose-based hydrogel composite that we developed here, are also attractive for therapeutic applications, particularly for inhibiting injury induced by reactive oxygen species (ROS), because of the scavenging ability of PB NPs toward ROS.[27] In conclusion, our approach opens up a new route for the development of integrated enzyme−nanozyme composite hydrogels, obtained from mild synthetic strategies, which can be implemented for different nanozymes and a wide range of potential biosensing applications.

■ ASSOCIATED CONTENT

Supporting Information

The Supporting Information is available free of charge at https://pubs.acs.org/doi/10.1021/acsanm.2c01609.

Optical microscopy, SEM, and TEM images of hydrogels, catalytic activity of PB−CMC and Fe−CMC toward H_2O_2, spectroscopic characterization of PB−CMC−GOx, colorimetric glucose detection with PB−CMC−GOx, and a comparison with other GOx−nanozyme composites (PDF)

■ AUTHOR INFORMATION

Corresponding Author

Marco Frasconi − *Department of Chemical Sciences, University of Padova, Padova 35131, Italy;* orcid.org/0000-0003-2010-175X; Email: marco.frasconi@unipd.it

Authors

Roberto Baretta − *Department of Chemical Sciences, University of Padova, Padova 35131, Italy*

https://doi.org/10.1021/acsanm.2c01609
ACS Appl. Nano Mater. 2022, 5, 13845−13853

Valeria Gabrielli − *Department of Chemical Sciences, University of Padova, Padova 35131, Italy*

Complete contact information is available at: https://pubs.acs.org/10.1021/acsanm.2c01609

Notes

The authors declare no competing financial interest.

■ ACKNOWLEDGMENTS

We thank Dr. Andrea Basagni (University of Padova) for carrying out SEM and PXRD analysis. This research was supported by the University of Padova under the 2019 STARS Grant programme "SensCo".

■ REFERENCES

(1) Vázquez-González, M.; Wang, C.; Willner, I. Biocatalytic Cascades Operating on Macromolecular Scaffolds and in Confined Environments. *Nat. Catal.* **2020**, *3*, 256−273.

(2) Zhang, X.; Li, G.; Chen, G.; Wu, D.; Wu, Y.; James, T. D. Enzyme Mimics for Engineered Biomimetic Cascade Nanoreactors: Mechanism, Applications, and Prospects. *Adv. Funct. Mater.* **2021**, *31*, 2106139.

(3) Lyu, Y.; Scrimin, P. Mimicking Enzymes: The Quest for Powerful Catalysts from Simple Molecules to Nanozymes. *ACS Catal.* **2021**, *11*, 11501−11509.

(4) Zheng, X.; Liu, Q.; Jing, C.; Li, Y.; Li, D.; Luo, W.; Wen, Y.; He, Y.; Huang, Q.; Long, Y.-T.; Fan, C. Catalytic Gold Nanoparticles for Nanoplasmonic Detection of DNA Hybridization. *Angew. Chem., Int. Ed.* **2011**, *50*, 11994−11998.

(5) Hu, Y.; Cheng, H.; Zhao, X.; Wu, J.; Muhammad, F.; Lin, S.; He, J.; Zhou, L.; Zhang, C.; Deng, Y.; Wang, P.; Zhou, Z.; Nie, S.; Wei, H. Surface-Enhanced Raman Scattering Active Gold Nanoparticles with Enzyme-Mimicking Activities for Measuring Glucose and Lactate in Living Tissues. *ACS Nano* **2017**, *11* (6), 5558−5566.

(6) Gao, L.; Zhuang, J.; Nie, L.; Zhang, J.; Zhang, Y.; Gu, N.; Wang, T.; Feng, J.; Yang, D.; Perrett, S.; Yan, X. Intrinsic Peroxidase-Like Activity of Ferromagnetic Nanoparticles. *Nat. Nanotechnol.* **2007**, *2*, 577−583.

(7) Dong, S.; Dong, Y.; Liu, B.; Liu, J.; Liu, S.; Zhao, Z.; Li, W.; Tian, B.; Zhao, R.; He, F.; Gai, S.; Xie, Y.; Yang, P.; Zhao, Y. Guiding Transition Metal-Doped Hollow Cerium Tandem Nanozymes with Elaborately Regulated Multi-Enzymatic Activities for Intensive Chemodynamic Therapy. *Adv. Mater.* **2022**, *34*, 2107054.

(8) Vázquez-González, M.; Liao, W.-C.; Cazelles, R.; Wang, S.; Yu, X.; Gutkin, V.; Willner, I. Mimicking Horseradish Peroxidase Functions Using Cu^{2+}-Modified Carbon Nitride Nanoparticles or Cu^{2+}-Modified Carbon Dots as Heterogeneous Catalysts. *ACS Nano* **2017**, *11* (3), 3247−3253.

(9) Ouyang, Y.; Biniuri, Y.; Fadeev, M.; Zhang, P.; Carmieli, R.; Vázquez-González, M.; Willner, I. Aptamer-Modified Cu^{2+}-Functionalized C-Dots: Versatile Means to Improve Nanozyme Activities-"Aptananozymes. *J. Am. Chem. Soc.* **2021**, *143* (30), 11510−11519.

(10) Xu, W.; Jiao, L.; Wu, Y.; Hu, L.; Gu, W.; Zhu, C. Metal−Organic Frameworks Enhance Biomimetic Cascade Catalysis for Biosensing. *Adv. Mater.* **2021**, *33*, 2005172.

(11) Wang, D.; Jana, D.; Zhao, Y. Metal−Organic Framework Derived Nanozymes in Biomedicine. *Acc. Chem. Res.* **2020**, *53* (7), 1389−1400.

(12) Wang, Q.; Zhang, X.; Huang, L.; Zhang, Z.; Dong, S. GOx@ZIF-8(NiPd) Nanoflower: An Artificial Enzyme System for Tandem Catalysis. *Angew. Chem., Int. Ed.* **2017**, *56*, 16082−16085.

(13) Cheng, X.; Zheng, Z.; Zhou, X.; Kuang, Q. Metal−Organic Framework as a Compartmentalized Integrated Nanozyme Reactor to Enable High-Performance Cascade Reactions for Glucose Detection. *ACS Sustainable Chem. Eng.* **2020**, *8* (48), 17783−17790.

(14) Zhong, X.; Xia, H.; Huang, W.; Li, Z.; Jiang, Y. Biomimetic Metal-Organic Frameworks Mediated Hybrid Multi-Enzyme Mimic for Tandem Catalysis. *Chem. Eng. J.* **2020**, *381*, 122758.

(15) Cai, X.; Jiao, L.; Yan, H.; Wu, Y.; Gu, W.; Du, D.; Lin, Y.; Zhu, C. Nanozyme-Involved Biomimetic Cascade Catalysis for Biomedical Applications. *Mater. Today* **2021**, *44*, 211−228.

(16) Zhu, H.; Liu, P.; Xu, L.; Wang, M.; Pan, J.; Niu, X. Emulsion-Templated Construction of Enzyme-Nanozyme Integrated Hierarchically Porous Hydrogels for Smartphone-Assisted Pesticide Biosensing. *Chem. Eng. J.* **2022**, *433*, 133669.

(17) Ballesteros, C. A.; Mercante, L. A.; Alvarenga, A. D.; Facure, M. H. M.; Schneider, R.; Correa, D. S. Recent Trends in Nanozymes Design: from Materials and Structures to Environmental Applications. *Mater. Chem. Front.* **2021**, *5*, 7419−7451.

(18) Li, Y.; Wang, D.; Wen, J.; Yu, P.; Liu, J.; Li, J.; Chu, H. Chemically Grafted Nanozyme Composite Cryogels to Enhance Antibacterial and Biocompatible Performance for Bioliquid Regulation and Adaptive Bacteria Trapping. *ACS Nano* **2021**, *15* (12), 19672−19683.

(19) Bulut, O.; Yilmaz, M. D. Catalytic Evaluation of Biocompatible Chitosan-Stabilized Gold Nanoparticles on Oxidation of Morin. *Carbohydr. Polym.* **2021**, *258*, 117699.

(20) Hao, Y.; Liu, Y.; Wu, Y.; Tao, N.; Lou, D.; Li, J.; Sun, X.; Liu, Y.-N. A Robust Hybrid Nanozyme@Hydrogel Platform as a Biomimetic Cascade Bioreactor for Combination Antitumor Therapy. *Biomater. Sci.* **2020**, *8*, 1830−1839.

(21) Wang, W.; Zheng, S.; Hong, Y.; Xu, X.; Feng, X.; Song, H. Hydrogel-Metal-Organic-Framework Nanoparticle Composites for Immobilization of Active Biomacromolecules. *ACS Appl. Nano Mater.* **2022**, *5*, 2222−2230.

(22) Huang, Y.; Ren, J.; Qu, X. Nanozymes: Classification, Catalytic mechanisms, Activity Regulation, and Applications. *Chem. Rev.* **2019**, *119* (6), 4357−4412.

(23) Zhu, X.; Mao, X.; Wang, Z.; Feng, C.; Chen, G.; Li, G. Fabrication of Nanozyme@DNA Hydrogel and Its Application in Biomedical Analysis. *Nano Res.* **2017**, *10* (3), 959−970.

(24) Tan, G.; Zhong, Y.; Yang, L.; Jiang, Y.; Liu, J.; Ren, F. A Multifunctional MOF-Based Nanohybrid as Injectable Implant Platform for Drug Synergistic Oral Cancer Therapy. *Chem. Eng. J.* **2020**, *390*, 124446.

(25) Vázquez-González, M.; Willner, I. Stimuli-Responsive Biomolecule-Based Hydrogels and Their Applications. *Angew. Chem., Int. Ed.* **2020**, *59* (36), 15342−15377.

(26) Ricci, F.; Palleschi, G. Sensor and Biosensor Preparation, Optimisation and Applications of Prussian Blue Modified Electrodes. *Biosens. Bioelectron.* **2005**, *21*, 389−407.

(27) Zhang, W.; Hu, S.; Yin, J. J.; He, W.; Lu, W.; Ma, M.; Gu, N.; Zhang, Y. Prussian Blue Nanoparticles as Multienzyme Mimetics and Reactive Oxygen Species Scavengers. *J. Am. Chem. Soc.* **2016**, *138*, 5860−5865.

(28) Vázquez-González, M.; Torrente-Rodriguez, R. M.; Kozell, A.; Liao, W.-C.; Cecconello, A.; Campuzano, S.; Pingarron, J. M.; Willner, I. Mimicking Peroxidase Activities with Prussian Blue Nanoparticles and Their Cyanometalate Structural Analogues. *Nano Lett.* **2017**, *17*, 4958−4963.

(29) Son, S. E.; Gupta, P. K.; Hur, W.; Choi, H.; Lee, H. B.; Park, Y.; Seong, G. H. Determination of Glycated Albumin Using a Prussian Blue Nanozyme-Based Boronate Affinity Sandwich Assay. *Anal. Chim. Acta* **2020**, *1134*, 41−49.

(30) María-Hormigos, R.; Molinero-Fernández, Á.; López, M. Á.; Jurado-Sánchez, B.; Escarpa, A. Prussian Blue/Chitosan Micromotors with Intrinsic Enzyme-like Activity for (bio)-Sensing Assays. *Anal. Chem.* **2022**, *94*, 5575−5582.

(31) Zhang, W.; Ma, D.; Du, J. Prussian Blue Nanoparticles as Peroxidase Mimetics for Sensitive Colorimetric Detection of Hydrogen Peroxide and Glucose. *Talanta* **2014**, *120*, 362−367.

(32) Bai, H.; Kong, F.; Feng, K.; Zhang, X.; Dong, H.; Liu, D.; Ma, M.; Liu, F.; Gu, N.; Zhang, Y. Prussian Blue Nanozymes Prevent Anthracycline-Induced Liver Injury by Attenuating Oxidative Stress

and Regulating Inflammation. *ACS Appl. Mater. Interfaces* **2021**, *13*, 42382−42395.
(33) Feng, K.; Zhang, J.; Dong, H.; Li, Z.; Gu, N.; Ma, M.; Zhang, Y. Prussian Blue Nanoparticles Having Various Sizes and Crystallinities for Multienzyme Catalysis and Magnetic Resonance Imaging. *ACS Appl. Nano Mater.* **2021**, *4*, 5176−5186.
(34) Hao, Y.; Mao, L.; Zhang, R.; Liao, X.; Yuan, M.; Liao, W. Multifunctional Biodegradable Prussian Blue Analogue for Synergetic Photothermal/Photodynamic/Chemodynamic Therapy and Intrinsic Tumor Metastasis Inhibition. *ACS Appl. Bio Mater.* **2021**, *4*, 7081−7093.
(35) Zhao, J.; Cai, X.; Gao, W.; Zhang, L.; Zou, D.; Zheng, Y.; Li, Z.; Chen, H. Prussian Blue Nanozyme with Multienzyme Activity Reduces Colitis in Mice. *ACS Appl. Mater. Interfaces* **2018**, *10*, 26108−26117.
(36) Cai, X.; Gao, W.; Zhang, L.; Ma, M.; Liu, T.; Du, W.; Zheng, Y.; Chen, H.; Shi, J. Enabling Prussian Blue with Tunable Localized Surface Plasmon Resonances: Simultaneously Enhanced Dual-Mode Imaging and Tumor Photothermal Therapy. *ACS Nano* **2016**, *10*, 11115−11126.
(37) Qin, Z.; Chen, B.; Mao, Y.; Shi, C.; Li, Y.; Huang, X.; Yang, F.; Gu, N. Achieving Ultrasmall Prussian Blue Nanoparticles as High-Performance Biomedical Agents with Multifunctions. *ACS Appl. Mater. Interfaces* **2020**, *12*, 57382−57390.
(38) Uemura, T.; Ohba, M.; Kitagawa, S. Size and surface effects of Prussian blue nanoparticles protected by organic polymers. *Inorg. Chem.* **2004**, *43*, 7339−7345.
(39) Eun, S.; Hong, H. J.; Kim, H.; Jeong, H. S.; Kim, S.; Jung, J.; Ryu, J. Prussian Blue-Embedded Carboxymethyl Cellulose Nanofibril Membranes for Removing Radioactive Cesium from Aqueous Solution. *Carbohydr. Polym.* **2020**, *235*, 115984.
(40) Rahman, M. S.; Hasan, M. S.; Nitai, A. S.; Nam, S.; Karmakar, A. K.; Ahsan, M. S.; Shiddiky, M. J. A.; Ahmed, M. B. Recent Developments of Carboxymethyl Cellulose. *Polymers* **2021**, *13* (8), 1345.
(41) Gabrielli, V.; Baretta, R.; Pilot, R.; Ferrarini, A.; Frasconi, M. Insights into the Gelation Mechanism of Metal-Coordinated Hydrogels by Paramagnetic NMR Spectroscopy and Molecular Dynamics. *Macromolecules* **2022**, *55*, 450−461.
(42) Zennifer, A.; Senthilvelan, P.; Sethuraman, S.; Sundaramurthi, D. Key Advances of Carboxymethyl Cellulose in Tissue Engineering & 3D Bioprinting Applications. *Carbohydr. Polym.* **2021**, *256*, 117561.
(43) Jaiswal, A. K.; Hokkanen, A.; Kapulainen, M.; Khakalo, A.; Nonappa; Ikkala, O.; Orelma, H. Carboxymethyl Cellulose (CMC) Optical Fibers for Environment Sensing and Short-Range Optical Signal Transmission. *ACS Appl. Mater. Interfaces* **2022**, *14* (2), 3315−3323.
(44) Orelma, H.; Filpponen, I.; Johansson, L.-S.; Laine, J.; Rojas, O. J. Modification of Cellulose Films by Adsorption of CMC and Chitosan for Controlled Attachment of Biomolecules. *Biomacromolecules* **2011**, *12*, 4311−4318.
(45) Orelma, H.; Teerinen, T.; Johansson, L.-S.; Holappa, S.; Laine, J. CMC-Modified Cellulose Biointerface for Antibody Conjugation. *Biomacromolecules* **2012**, *13*, 1051−1058.
(46) Lichtenberg, J. Y.; Ling, Y.; Kim, S. Non-Specific Adsorption Reduction Methods in Biosensing. *Sensors* **2019**, *19* (11), 2488.
(47) Swoboda, B. E. P.; Massey, V. Purification and Properties of the Glucose Oxidase from Aspergillus Niger. *J. Biol. Chem.* **1965**, *240*, 2209−2215.
(48) Li, N.; Chen, G.; Chen, W.; Huang, J.; Tian, J.; Wan, X.; He, M.; Zhang, H. Multivalent Cations-Triggered Rapid Shape Memory Sodium Carboxymethyl Cellulose/Polyacrylamide Hydrogels with Tunable Mechanical Strength. *Carbohydr. Polym.* **2017**, *178*, 159−165.
(49) Fu, G.; Liu, W.; Feng, S.; Yue, X. Prussian Blue Nanoparticles Operate as a New Generation of Photothermal Ablation Agents for Cancer Therapy. *Chem. Commun.* **2012**, *48*, 11567−11569.
(50) Zheng, S. Y.; Ding, H.; Qian, J.; Yin, J.; Wu, Z. L.; Song, Y.; Zheng, Q. Metal-Coordination Complexes Mediated Physical Hydrogels with High Toughness, Stick−Slip Tearing Behavior, and Good Processability. *Macromolecules* **2016**, *49* (24), 9637−9646.
(51) Hu, M.; Furukawa, S.; Ohtani, R.; Sukegawa, H.; Nemoto, Y.; Reboul, J.; Kitagawa, S.; Yamauchi, Y. Synthesis of Prussian Blue Nanoparticles with a Hollow Interior by Controlled Chemical Etching. *Angew. Chem., Int. Ed.* **2012**, *51*, 984−988.
(52) Wilde, R. E.; Ghosh, S. N.; Marshall, B. J. The Prussian Blues. *Inorg. Chem.* **1970**, *9* (11), 2512−2516.
(53) Buser, H. J.; Schwarzenbach, D.; Petter, W.; Ludi, A. The Crystal Structure of Prussian Blue: $Fe_4[Fe(CN)_6]_3.xH_2O$. *Inorg. Chem.* **1977**, *16*, 2704−2710.
(54) Kremer, M. L. Mechanism of the Fenton Reaction. Evidence for a New Intermediate. *Phys. Chem. Chem. Phys.* **1999**, *1*, 3595−3605.
(55) Su, L.; Xiong, Y.; Yang, H.; Zhang, P.; Ye, F. Prussian Blue Nanoparticles Encapsulated Inside a Metal−Organic Framework via in Situ Growth as Promising Peroxidase Mimetics for Enzyme Inhibitor Screening. *J. Mater. Chem. B* **2016**, *4*, 128−134.
(56) Park, J. S.; Choi, J. S.; Han, D. K. Platinum Nanozyme-Hydrogel Composite (PtNZHG)-Impregnated Cascade Sensing System for One-Step Glucose Detection in Serum, Urine, and Saliva. *Sens. Actuators B* **2022**, *359*, 131585.